PCCP

PAPER

View Article Online
View Journal | View Issue

Cite this: *Phys. Chem. Chem. Phys.*, 2019, **21**, 9069

Triangular graphene nanofragments: open-shell character and doping†

María E. Sandoval-Salinas,[ab] Abel Carreras[b] and David Casanova*[b]

Received 1st February 2019,
Accepted 4th March 2019

DOI: 10.1039/c9cp00641a

rsc.li/pccp

In this work we study the intricacies of the electronic structure properties of triangular graphene nanofragments (TGNFs) in their ground and low-lying excited states by means of *ab initio* quantum chemistry calculations. We focus our attention on the radical and diradical characters of phenalenyl and triangulene, the smallest members of the TGNF family, and we describe the nature of their low-lying excited states. Moreover, we rationalize the modulation of the electronic and magnetic properties by means of selective boron or nitrogen substitution of carbon sites and by hydrogen saturation. The obtained results aim to guide future design of graphene-based materials with well-defined properties.

1 Introduction

Nowadays, graphene based materials are exhaustively studied theoretically and experimentally due to their potential application as main components in molecular electronics[1] and spintronic devices.[2] Graphene is a two-dimensional arrangement of sp^2 carbons arising from the fusion of benzene rings. It is a strongly diamagnetic material and its electronic structure shows a zero-bandgap. On the other hand, the quantum confinement of finite sheets of fused π-conjugated hexagonal rings within the nanoscale, *i.e.* graphene nanofragments (GNFs), breaks the degeneracy between conduction and valence bands at the Dirac points and the gap between the occupied and virtual levels opens, while molecular like electronic properties emerge. Historically, compounds sharing honeycomb conformations of carbon atoms have been considered as derivatives of graphene, such as buckyballs, tubes, sheets and multidimensional graphene-fragments (0D, 1D and 2D; and 3D structures obtained as stacked graphene layers). In particular, finite 2D graphene fragments are known as nanoflakes or nanofragments,[3,4] and this is the nomenclature that we use here.

The optoelectronic and magnetic properties of GNFs strongly depend on their size, shape and topology. Many of these graphene motifs present closed-shell electronic structures, while some of them possess a high-spin ground state.[5] This is the case of non-Kekulé polyaromatic hydrocarbons (PAHs),[6] such as triangular GNFs (TGNFs), which have been categorized as open-shell graphene fragments. The π-electron conjugation character of the states around the Fermi level in these systems induces a rather delocalized radical character that makes them potential building blocks for the design of new materials with the possibility of long-range interactions between unpaired spins.

In the past, the lack of efficient synthetic routes for their preparation and their rather weak stability have been major impediments for the practical use of radical and poly-radical TGNFs,[7–9] but more recently such limitations have been largely overcome through chemical functionalization of TGNF edges, and through what has been described as synthetic organic spin chemistry.[10,11] Rather recently, stable phenalenyl and triangulene derivatives with variable radical characters have been synthesized and characterized showing very interesting redox, magnetic and electronic properties.[12,13] Besides, the characterization of small molecular systems can be used to understand and rationalize the characteristics of larger graphene nanostructures, such as nanoribbons,[14] or TGNF aggregates.[11,15]

The spin multiplicity of PAHs can be predicted by a simple Ovchinnikov's rule,[16] rigorously established by Lieb's theorem for bipartite lattices,[17] and based on the antiferromagnetic nature of the spin–spin interaction of the chemical bond. The rule attributes the preferred spin of the ground state as half of the difference between the number of carbon atoms belonging to opposite sublattices, also referred to as atomic sites with different colors. In spite of the simplicity of the rule, as far as we know, there are no counter examples of its validity in the determination of the most stable spin state in planar alternant conjugated hydrocarbons. The electronic structure properties of TGNFs have been theoretically described and computationally explored at different approximation levels, from thigh-binding models,[18–21] density functional theory (DFT),[4,22–25] to multi-reference correlation methods.[26–29]

The electronic and magnetic properties of graphene and GNFs can be further modified through heteroatom substitution

[a] *Departament de Ciència de Materials i Química Física and Institut de Química Teòrica i Computacional (IQTCUB) Universitat de Barcelona, Martí i Franquès 1-11, Barcelona, Catalunya, 08028, Spain*
[b] *Donostia International Physics Center (DIPC), Paseo Manuel de Lardizabal 4, 20018 Donostia, Euskadi, Spain. E-mail: david.casanova@ehu.eus*

† Electronic supplementary information (ESI) available. See DOI: 10.1039/c9cp00641a

of carbon sites.[30,31] Precise and controlled n-type or p-type doping in graphene is a well-known strategy for engineering the Fermi level in the design of new materials with improved properties. Experimental methods devoted to the controlled substitution of carbon atoms by other species have appeared and been developed since the early studies on graphene, especially in the synthesis of N- and B-doped graphene.[32–36] Interestingly, the electronic structure characteristics of these compounds depend not only on the dopant concentration, but also on the doping symmetry pattern.[37]

In the present study we aim to describe the electronic structure properties of the ground and low-lying excited states of pristine and doped TGNFs. We focus our attention on the investigation of the smallest elements within the TGNF family, *i.e.* phenalenyl (**1**) and triangulene (**2**), and some of their derivatives obtained through B- and N-substitution, and by hydrogenation (Fig. 1). To this end, we employ high-level electronic structure methodologies to rationalize the relative stability of electronic states with different spin multiplicities, combined with computational tools to characterize their radical or poly-radical character.

2 Computational details

Molecular geometries have been optimized within the density functional theory (DFT) with the M06-2X exchange–correlation functional[38] and the 6-311G(d,p) basis set. The potential presence of strong electronic correlations in the studied TGNFs recommends the use of quantum chemistry models able to capture the multiconfigurational character of the electronic states. Therefore, ground and low-lying excited electronic states have been computed with the same basis set and by means of the restricted active space configuration interaction (RASCI)[39–41] with the hole and electron approximation and the use of a spin–flip excitation operator (promotion of α electrons into empty β orbitals). This methodology represents a well-balanced and computationally affordable approach for the study of ground and low-lying states of strongly correlated molecular systems, and has shown to be very reliable in the description of the electronic structure of PAHs with di- and poly-radical characters.[42–49] Detailed description of the orbital spaces employed for each system can be found in the ESI† (Table S1). The radical and poly-radical characters of electronic states have been evaluated through the representation of natural orbitals and the fractional occupation density (FOD):[50,51]

$$\rho_{\mathrm{FOD}}(\mathbf{r}) = \sum_i (1 - \mathrm{abs}(1 - n_i))|\phi_i(\mathbf{r})|^2 \quad (1)$$

where n_i is the electron occupancy of the ith natural orbital $\phi_i(\mathbf{r})$. The number of unpaired electrons has been quantified by the (linear) Head-Gordon N_{U} metrics[52] (eqn (2)). It is noted that the integration of the FOD over the entire space is equivalent to N_{U}.

$$N_{\mathrm{U}} = \sum_i (1 - \mathrm{abs}(1 - n_i)) \quad (2)$$

All calculations have been performed with the Q-Chem package.[53]

3 Pristine compounds

The phenalenyl free radical (**1**) is the smallest graphene triangular nanoflake, built as three fused benzene rings sharing a central carbon atom, and with a planar structure belonging to the D_{3h} symmetry point group. Molecule **1** has an odd number of sp^2 carbon atoms with 13 π-electrons, inevitably resulting in a radical system. The ground state spin-multiplicity predicted by the Hückel model exhibits one unpaired electron (Fig. 2), *i.e.* the $1^2A_1'$ state, in agreement with Ovchinnikov's rule. The next triangular PAH is triangulene (**2**), which can be seen as the fusion of three additional benzene rings to **1** preserving the D_{3h} symmetry. Molecule **2** contains an even number of π-electrons with a spin-triplet ground state ($1^3A_1'$), as predicted by Ovchinnikov's rule and the Hückel

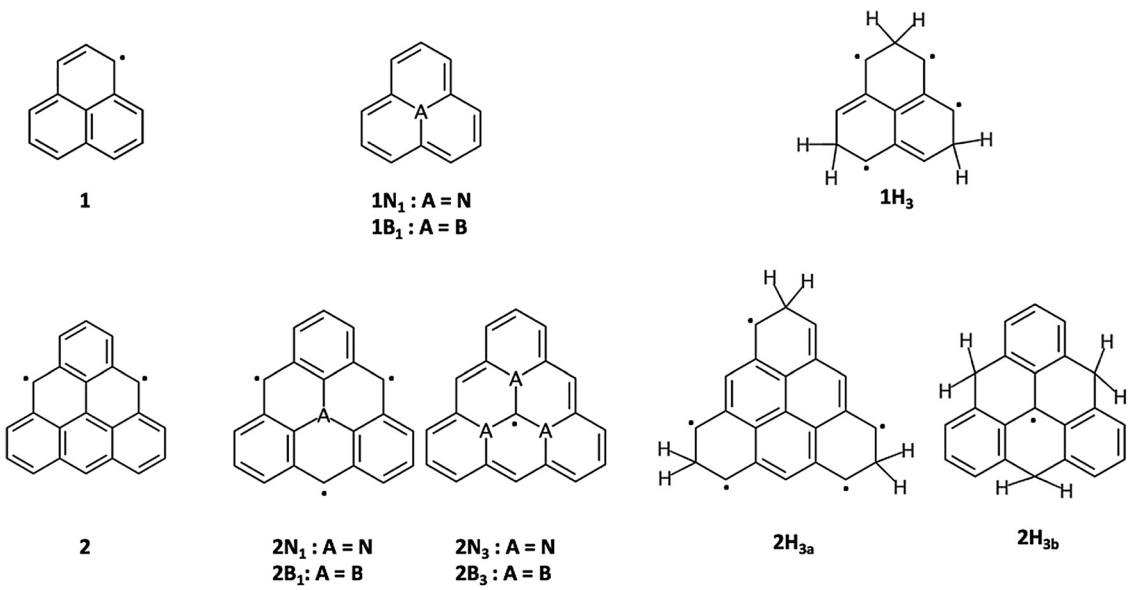

Fig. 1 Pristine phenalenyl (**1**), triangulene (**2**), and their B- and N-doped and hydrogenated derivatives.

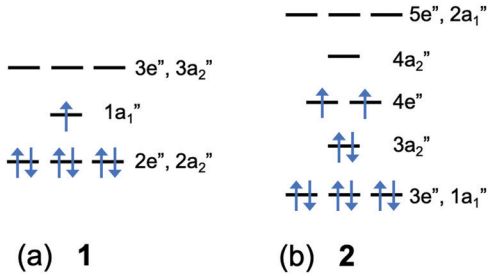

Fig. 2 Hückel MO energy diagram of (a) phenalenyl (**1**) and (b) triangulene (**2**).

model (Fig. 2), and confirmed through ESR spectroscopy.[6,11] It is noted that both frontier molecular orbital diagrams obtained by the Hückel scheme present degeneration degrees beyond the one dictated by the molecular D_{3h} symmetry, with sets of triply degenerated π-orbitals. Such degeneration is triggered by the molecular topology within the Hückel model and is lifted when performing *ab initio* calculations.

The $2p_z$ orbital on the central carbon atom of **1** and **2** belongs to the A_2'' irreducible representation. Therefore, the atom in the molecular center can only contribute to π-orbitals with that symmetry, *i.e.* a_2'' orbitals (Fig. 2). The electronic occupation of Hückel π-orbitals predicts the lack of unpaired electron density on the central atom. Correlated electronic structure calculations further characterize the ground state radical nature of **1** and **2**, with the unpaired electron density localized on the molecular edges and natural orbital occupancies corresponding to doublet and triplet states, respectively (Fig. 3 and Fig. S1, ESI†).

The lowest-lying excited states of **1** correspond to $1^2E''$ and $1^2A_2''$, obtained as ($\pi \rightarrow \pi^*$) $2e'' \rightarrow 1a_1''$ and $2a_2'' \rightarrow 1a_1''$ electronic promotions, respectively. The vertical energy gaps are computed at 2.76 and 3.04 eV, respectively (Table 1), in excellent agreement with multireference CI (MR-CI) energies.[29] Therefore, while the doubly degenerated $1^2E''$ transitions correspond to the excitation of edge electrons, the $1^2A_2''$ state contains a partial displacement of central electrons to the molecular contour.

The single electron occupation of the $4e''$ orbitals in **2** results in a four dimensional space with A_1', A_2' and E' symmetries. The anti-symmetric spatial representation component of the direct product $E'' \otimes E''$ corresponds to the ground state triplet ($1^3A_2'$), while the A_1' and E' are linked to spin-singlet excited states (Table 1). The energy gap to the lowest excited singlet of **2** ($1^1E'$) is computed at 0.57 eV.

The doubly degenerated singlet is obtained mainly as the combination of single electron occupation of $4e''$ orbitals, hence also exhibiting a fractional occupation density localized on the molecular edges. The triplet–triplet transition energy to the first excited triplet of **2** ($1^3E'$) is computed at 2.82 eV and involves electronic configurations with the partial occupation of the $3a_2''$ and $4a_2''$ orbitals.

Table 1 Low-lying states of **1** and **2**, energy gaps (in eV) and unpaired electron numbers (N_U) computed at the RAS-SF/6-311G(d,p) level

Mol.	State	ΔE	N_U
1	$1^2A_1''$	—	1.58
	$1^2E_2''$	2.76	2.68
	$1^2A_2''$	3.04	1.99
2	$1^3A_2'$	—	2.53
	$1^1E'$	0.57	2.52
	$1^3E'$	2.82	3.44

4 B-Doped and N-doped TGNFs

In the following, we explore the role of atomic doping on the electronic properties of TGNFs by replacing inner carbon atoms of **1** and **2** by boron or nitrogen, *i.e.* electron-donating or electron-accepting elements, respectively.

4.1 Phenalenyl derivatives

First we consider B-doped and N-doped phenalenyl resulting from the substitution of the central carbon atom (Fig. 1). The replacement of the central carbon atom by one boron or nitrogen modifies the number of π-electrons of the molecule, and the application of Ovchinnikov's rule to $\mathbf{1B}_1$ and $\mathbf{1N}_1$, that is removing the central site in the evaluation of carbon atoms belonging to opposite sublattices, predicts the ground state spin-singlet systems. But such simplification cannot account for the electronic structure details of the doped systems, such as the diradical (or diradicaloid) character of the molecule dictated by the gap between occupied and virtual orbitals. Since the $2p_z$ orbital of boron (nitrogen) is higher (lower) in energy than the carbon's counterpart, the a_2'' frontier π MOs are destabilized (stabilized) in $\mathbf{1B}_1$ ($\mathbf{1N}_1$), as obtained by the Hückel model (Fig. 4). The energy shift of a_2'' orbitals might eventually

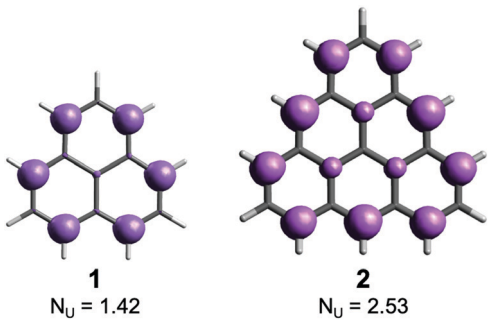

Fig. 3 Ground state fractional occupied density (FOD) of **1** and **2**.

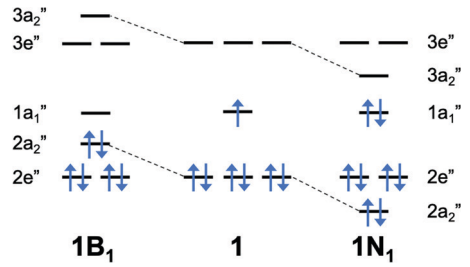

Fig. 4 Hückel MO energy diagram B-doped ($\mathbf{1B}_1$) and N-doped ($\mathbf{1N}_1$) at the central atom position compared to pristine **1**.

Table 2 Low-lying states of $\mathbf{2B_1}$ and $\mathbf{2N_1}$, energy gaps (in eV) and unpaired electron numbers (N_U) computed at the RAS-SF/6-311G(d,p) level

Mol.	State	ΔE	N_U
$\mathbf{1B_1}$	$1^1A_1'$	—	0.63
	$1^1A_2'$	0.66	2.40
	$1^3A_2'$	0.79	2.36
$\mathbf{1N_1}$	$1^1A_1'$	—	0.55
	$1^1A_2'$	0.85	2.40
	$1^3A_2'$	0.96	2.36

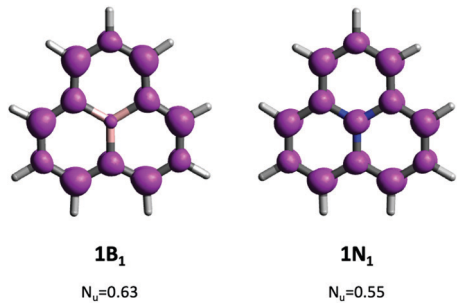

Fig. 5 Ground state fractional occupied density (FOD) of $\mathbf{1B_1}$ and $\mathbf{1N_1}$.

result in small HOMO-to-LUMO energy gaps inducing an open-shell character to the ground state wave function.

The molecular geometries at the ground state ($1^1A_1'$) of $\mathbf{1B_1}$ and $\mathbf{1N_1}$ preserve the D_{3h} symmetry, with slight changes on the bond distances, *i.e.* shorter B–C and longer N–C bond distances than the C–C ones at the center of **1** (Fig S2, ESI†). The electronic structure calculations confirm the ground state spin-singlet nature of $\mathbf{1B_1}$ and $\mathbf{1N_1}$, and predict singlet–triplet energy differences smaller than 1 eV (Table 2). The energy gap to the lowest triplet state is an indirect measure of the open-shell character of molecular ground state singlets, with smaller gaps corresponding to stronger diradical nature. Both doped derivatives show moderate diradical (or diradicaloid) characters, approximately corresponding to half unpaired electrons as measured by N_U. In both cases, the unpaired electron density emerges, for the most part, from the fractional occupation of the a_1'' and a_2'' orbitals, which results in a different distribution with respect to the pristine **1** (mainly corresponding to the single electron occupation of $1a_1''$). The moderate amount of unpaired electrons is almost equally distributed between all contour carbons with contributions from the central doping atom, especially in $\mathbf{1N_1}$ (Fig. 5).

The lowest excited singlet state of the doped phenalenyl is obtained as the HOMO-to-LUMO single electron excitation and belongs to the same spatial symmetry as the lowest triplet. The energy of $1^1A_2'$ is systematically computed as $\sim$0.1 eV below $1^3A_2'$, which can be rationalized as a result of a small exchange integral between the a_1'' and a_2'' frontier orbitals due to their poor spatial overlap, and the larger capacity of the singlet state to mix with other open-shell electronic configurations (see the ESI†).

4.2 Triangulene derivatives

The boron and nitrogen mono-substituted $\mathbf{2B_1}$ and $\mathbf{2N_1}$ derivatives hold odd numbers of π-electrons. The computational results at the M06-2X level indicate a doublet ground state with adiabatic energy gaps to the quartet state (ΔE_{DQ}^{ad}) of 4.2 and 11.2 kcal mol^{-1} respectively, in disagreement with Ovchinnikov's rule, which predicts a preference for the spin-quartet multiplicity.

Stabilization of the doublet state in $\mathbf{2B_1}$ and $\mathbf{2N_1}$ is driven by a Jahn–Teller distortion[54–56] that lowers the molecular symmetry to C_{2v}. The existence of a third order symmetry axis in TGNFs induces the presence of two-fold degenerate electronic terms E, which are prompt to instabilities with respect to nuclear displacements that lower the symmetry and remove the degeneracies.[57] At the D_{3h} molecular symmetry the high-spin quartet of both mono-doped species, obtained as the single electron occupation of a_2'' and e'' orbitals ($^4A_2''$), lies slightly above the two-folded doublet $^2E''$ state (Table 3). But the D_{3h} arrangement is unstable upon certain structural deformations. The Jahn–Teller active distortion modes able to split the doublet state must be different from the totally symmetric representation and must be contained in the symmetric contribution of the direct self-product of the E″ representation. Therefore, the Jahn–Teller distortions able to break the degeneracy of $^2E''$ states must follow an $S(e')$ mode (Fig. 6).

Structure modification upon the action of the $S(e')$ vibration breaks the degeneracy of e'' orbitals and allows e''/a_2'' orbital mixing (Fig. 7). As a result, the doublet configuration is stabilized in the C_{2v}

Table 3 Vertical energy gaps (in eV) between low-lying states with different spin-multiplicities and unpaired electron numbers (N_U) of B- and N-doped triangulene derivatives computed at the RAS-SF/6-311G(d,p) level

Mol.	Sym.	State	ΔE	N_U
$\mathbf{2B_1}$	D_{3h}	$1^2E''$	—	1.58
		$1^4E_2''$	0.15	3.03
$\mathbf{2B_1}$	C_{2v}	1^2B_2	—	1.47
		1^4A_2	0.32	3.03
$\mathbf{2N_1}$	D_{3h}	$1^2E''$	—	1.50
		$1^4A_2''$	0.06	3.02
$\mathbf{2N_1}$	C_{2v}	1^2B_2	—	1.49
		1^4A_2	0.25	3.02
$\mathbf{2B_3}$	D_{3h}	$1^2A_2''$	—	2.99
		$1^4A_2''$	1.40	3.25
$\mathbf{2N_3}$	D_{3h}	$1^2A_2''$	—	2.77
		$1^4A_2''$	2.06	4.72
$\mathbf{2N_2}$	C_{2v}	1^1A_1	—	0.20
		1^3B_1	2.30	2.11

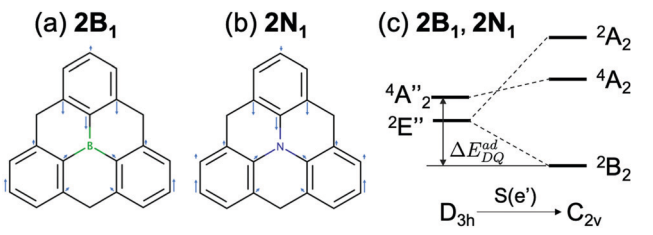

Fig. 6 Qualitative representation of the $S(e')$ distortion between the optimized geometries of the quartet (D_{3h}) and doublet (C_{2v}) optimized geometries of $\mathbf{2B_1}$ (a) and $\mathbf{2N_1}$ (b), and (c) state diagram for the two molecular symmetries.

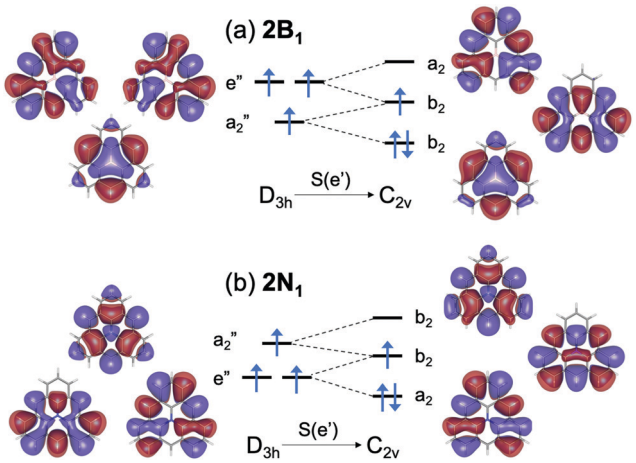

Fig. 7 MO energy diagram of $\mathbf{2B_1}$ (a) and $\mathbf{2N_1}$ (b) of mono-doped triangulenes for the D_{3h} and C_{2v} molecular symmetries. Represented MOs correspond to M06-2X α-spin orbitals.

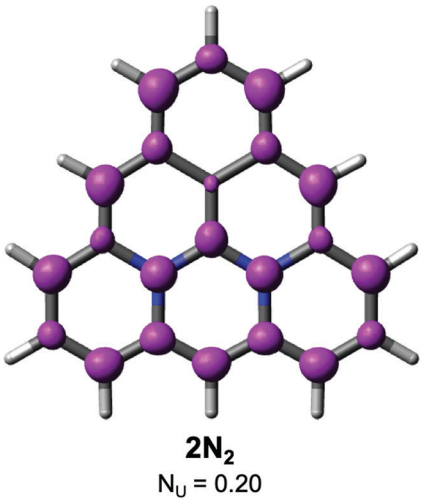

Fig. 9 Ground state fractional occupied density (FOD) of $\mathbf{2N_2}$.

geometry with the unpaired electron occupying a b_2-orbital. Moreover, the vertical gap to the spin-quartet state of $\mathbf{2B_1}$ and $\mathbf{2N_1}$ sensibly increases upon the $S(e')$ distortion towards the C_{2v} geometry.

Accordingly, while the unpaired electrons of the high-spin state symmetrically delocalize over the entire π-system, the unpaired electron density of the ground state doublet (1^2B_2) in the mono-substituted triangulenes does not preserve the three fold symmetry axis and delocalizes on one of the triangle edges of $\mathbf{2B_1}$ and at one of the vertices in $\mathbf{2N_1}$ (Fig. 8).

Equivalently, the action of e′-symmetry Jahn–Teller distortion modes on **2** results in the splitting of the lowest $^1E'$ state. But, contrary to the situation in $\mathbf{2B_1}$ and $\mathbf{2N_1}$, such stabilization is not enough for the lowest spin-state to become the global minimum of the system ($\Delta E_{ST}^{ad} = -8.6$ kcal mol^{-1}).

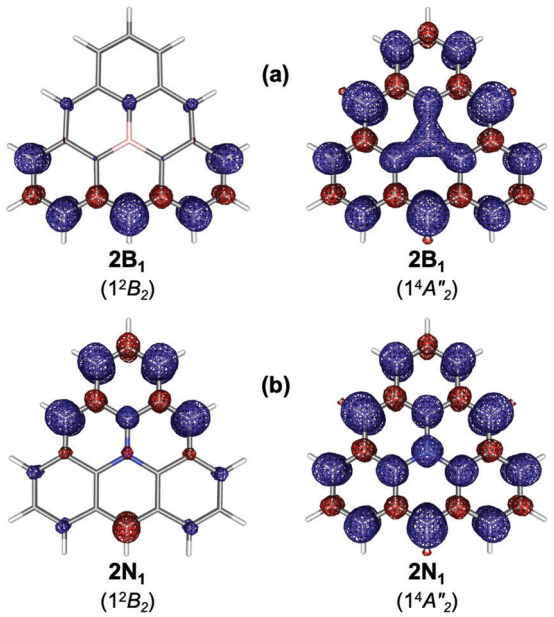

Fig. 8 Spin densities of 1^2B_2 (C_{2v}) and $1^4A_2''$ (D_{3h}) states of $\mathbf{2B_1}$ (a) and $\mathbf{2N_1}$ (b) in their respective optimized geometries.

The C_3-symmetric substitution of three carbon atoms by boron or nitrogen respectively in $\mathbf{2B_3}$ and $\mathbf{2N_3}$ stabilizes the low-spin doublet state. Contrary to the mono-substituted species, $\mathbf{2B_3}$ and $\mathbf{2N_3}$ keep the overall D_{3h} molecular symmetry, since the unpaired electron lies on a (non-degenerated) a_2''-orbital. The characterization of their ground state radical character identifies one unpaired electron mainly localized on the central atom with small C_3-symmetrical contributions from the doping atoms and the carbons at the center of the triangle edges (Fig. S6, ESI†). The computed energy gaps to the quartet state are shown in Table 3.

Finally, we consider the non-symmetric N-doping of **2** by replacing two inner carbon atoms ($\mathbf{2N_2}$), for which the substitution pattern already reduces the molecular symmetry to C_{2v}. The connectivity between the carbon atoms sensibly stabilizes the closed-shell configuration, resulting in a spin-singlet ground state with a weak diradical character identified by a quite small N_U value. Similarly to pristine triangulene, the unpaired electron density of $\mathbf{2N_2}$ locates on the molecular edges, although it also exhibits a radical character on the two doping atoms (Fig. 9). The small diradical character of $\mathbf{2N_2}$ is in agreement with the computed rather large gap to the lowest triplet state.

5 Hydrogenated TGNF

The selective hydrogen saturation of peripheral carbon positions following Ovchinnikov's rule has been shown to be a simple and effective strategy in order to design high-spin states of PAHs.[27] Here we symmetrically convert three sp^2 carbons of **1** and **2** molecules into sp^3 sites (Fig. 1).

The saturation of the three corners of **1** results in a triallylmethane type product in which the sp^3 atoms enforce molecular planarity with a D_{3h} symmetry. The topology of the sp^2 sites in $\mathbf{1H_3}$ favors the high-spin stabilization, and its ground state corresponds to a spin-quintet ($1^5A_1'$) state. The unpaired electron density at the ground state is distributed amongst the sp^2 atoms bonded to the CH_2 fragments and the central atom (Fig. S7, ESI†). The lowest doubly degenerated triplet and

Table 4 Vertical energy gaps (in eV) between the low-lying states with different spin-multiplicities and unpaired electron numbers (N_U) of H-saturated **1** and **2** derivatives computed at the RAS-SF/6-311G(d,p) level

Mol.	Sym.	State	ΔE	N_U
$\mathbf{1H}_3$	D_{3h}	$1^5A_2'$	—	4.16
		$1^3E'$	0.40	4.09
		$1^1E'$	1.11	4.05
$\mathbf{2H}_{3a}$	D_{3h}	$1^6A_2''$	—	5.28
		$1^4E''$	0.26	4.79
		$1^2E''$	0.66	4.60
$\mathbf{2H}_{3b}$	D_{3h}	$1^2A_2''$	—	1.29
		$1^2E''$	3.16	1.82

singlet states lie at 0.40 and 1.11 eV above the high-spin ground state, in very good agreement with accurate correlated *ab initio* and spin decontamination corrections of DFT energies (Table 4).[27]

Similarly, hydrogenation of the corner carbon atoms of **2** in $\mathbf{2H}_{3a}$ results in a high-spin ground state with five unpaired electrons, and with energy gaps to lower spin-multiplicities resulting from the spin–flip of one and two electrons of 0.26 and 0.66 eV, respectively. Contrarily, three-folded saturation of **2** at the center of the triangle edges ($\mathbf{2H}_{3b}$) reduces the imbalance between the number of carbons in each of the two sublattices, which stabilizes the low-spin (doublet) state.

6 Conclusions

We have employed DFT calculations and a correlated wave function method combined with different computational techniques to describe in great detail the electronic structure properties of small TGNFs. The pristine phenalenyl molecule is a doublet state with a radical character arising from the single electron occupation of an a_1'' orbital delocalized at the molecular edges. Similarly, the radical character of the ground state triplet of triangulene is located at the carbon edges with no participation of the central and vertex sites.

Substitution of carbon atoms by boron or nitrogen can be used to tune the electronic and magnetic properties of TGNFs. Although in the present study we have not systematically explored all possible doping patterns, the obtained results predict that, in general, B and N doping of GNFs tends to stabilize the lowest-spin states and reduce the poly-radical character with respect to the unsubstituted counterparts. The substitution symmetry pattern dictates the distribution of unpaired electrons and can be used to design TGNF ensembles with the desired properties. Unexpectedly, the fractional occupation of the degenerated levels induces a Jahn–Teller distortion of mono-doped triangulene resulting in the stabilization of the doublet state, which cannot be taken into account by simple models such as Lieb's theorem. Hence, these results show that the generalization of Ovchinnikov's rule in doped GNFs has to be taken with precaution when replacing carbon sites by B or N atoms, which in Ovchinnikov's rule corresponds to removing the doped site of the sublattice. Since the 2p levels of boron and nitrogen are energetically close to those of the carbon atom, they can interact with the π-system of the molecule and modify their electronic properties. Selective saturation of the carbon edge positions of **1** and **2** has a very strong impact on the ground state spin multiplicity, and hence their magnetic properties.

These results can be extended to understand the poly-radical character in larger TGNFs, expected to be localized on the molecular edges of pristine TGNFs, and their derivatives. Moreover, heteroatom doping can be used to tune electronic and magnetic properties.

Conflicts of interest

There are no conflicts to declare.

Acknowledgements

The authors knowledge financial support from the Spanish Government MINECO/FEDER (project CTQ2016-80955-P). M. E. S.-S. acknowledges CONACYT-México for a PhD fellowship (ref. 591700). The authors are thankful for the technical and human support provided by the Donostia International Physics Center (DIPC) Computer Center, as well as by IZO-SGI SGIker at the University of the Basque Country (UPV/EHU).

References

1 B. Feringa, *Molecular Switches*, Wiley, 2001.
2 W. Han, R. K. Kawakami, M. Gmitra and J. Fabian, Graphene spintronics, *Nat. Nanotechnol.*, 2014, **9**, 794.
3 A. K. Geim and K. S. Novoselov, The rise of graphene, *Nat. Mater.*, 2007, **6**, 183–191.
4 W. L. Wang, S. Meng and E. Kaxiras, Graphene NanoFlakes with Large Spin, *Nano Lett.*, 2008, **8**, 241–245.
5 R. C. Haddon, Design of organic metals and superconductors, *Nature*, 1975, **256**, 394–396.
6 J. Inoue, K. Fukui, T. Kubo and S. Nakazawa, The First Detection of a Clar's Hydrocarbon, Triplet of Non-Kekulé Polynuclear Benzenoid Hydrocarbon, *J. Am. Chem. Soc.*, 2001, **123**, 12702–12703.
7 E. Clar, *The Aromatic Sextet*, Wiley, New York, NY, 1972.
8 E. Clar and D. G. Stewart, Aromatic Hydrocarbons. LXV. Triangulene Derivatives1, *J. Am. Chem. Soc.*, 1953, **75**, 2667–2672.
9 G. Allinson, R. J. Bushby, M. V. Jesudason, J.-L. Paillaud and N. Taylor, The synthesis of singlet ground state derivatives of non-Kekulé polynuclear aromatics, *J. Chem. Soc., Perkin Trans. 2*, 1997, 147–156.
10 R. Hicks, *Stable Radicals: Fundamentals and Applied Aspects of Odd-Electron Compounds*, Wiley, 2011.
11 Y. Morita, S. Suzuki, K. Sato and T. Takui, Synthetic organic spin chemistry for structurally well-defined open-shell graphene fragments, *Nat. Chem.*, 2011, **3**, 197–204.
12 A. Ueda, H. Wasa, S. Nishida, Y. Kanzaki, K. Sato, D. Shiomi, T. Takui and Y. Morita, An Extremely Redox-Active Air-Stable Neutral π Radical: Dicyanomethylene-Substituted Triangulene with a Threefold Symmetry, *Chem. – Eur. J.*, 2012, **18**, 16272–16276.
13 P. Ribar, T. Šolomek, L. Le Pleux, D. Häussinger, A. Prescimone, M. Neuburger and M. Jurček, Donor–Acceptor Molecular Triangles, *Synthesis*, 2017, 899–909.

14 J. Liu, B.-W. Li, Y.-Z. Tan, A. Giannakopoulos, C. Sanchez-Sanchez, D. Beljonne, P. Ruffieux, R. Fasel, X. Feng and K. Müllen, Toward Cove-Edged Low Band Gap Graphene Nanoribbons, *J. Am. Chem. Soc.*, 2015, **137**, 6097–6103.
15 Z.-h. Cui, A. Gupta, H. Lischka and M. Kertesz, Concave or convex π-dimers: the role of the pancake bond in substituted phenalenyl radical dimers, *Phys. Chem. Chem. Phys.*, 2015, **17**, 23963–23969.
16 A. A. Ovchinnikov, Multiplicity of the ground state of large alternant organic molecules with conjugated bonds, *Theor. Chim. Acta*, 1978, **47**, 297–304.
17 E. H. Lieb, Two theorems on the Hubbard model, *Phys. Rev. Lett.*, 1989, **62**, 1201–1204.
18 Y. Hancock, A. Uppstu, K. Saloriutta, A. Harju and M. J. Puska, Generalized tight-binding transport model for graphene nanoribbon-based systems, *Phys. Rev. B: Condens. Matter Mater. Phys.*, 2010, **81**, 245402.
19 A. Monari and S. Evangelisti, *Finite-Size Effects in Graphene Nanostructures*, 2011.
20 A. V. Luzanov, F. Plasser, A. Das and H. Lischka, Evaluation of the quasi correlated tight-binding (QCTB) model for describing polyradical character in polycyclic hydrocarbons, *J. Chem. Phys.*, 2017, **146**, 064106.
21 J. Li, S. Sanz, M. Corso, D. J. Choi, D. Peña, T. Frederiksen and J. I. Pascual, Single spin localization and manipulation in graphene open-shell nanostructures, *Nat. Commun.*, 2019, **10**, 200.
22 M. R. Philpott, F. Cimpoesu and Y. Kawazoe, Geometry, bonding and magnetism in planar triangulene graphene molecules with D_{3h} symmetry: zigzag $C_{m^{**}2+4m+1}H_{3m+3}$ (m = 2,. . .,15), *Chem. Phys.*, 2008, **354**, 1–15.
23 J. Fernández-Rossier and J. J. Palacios, Magnetism in Graphene Nanoislands, *Phys. Rev. Lett.*, 2007, **99**, 177204.
24 T. Yamamoto, T. Noguchi and K. Watanabe, Edge-state signature in optical absorption of nanographenes: tight-binding method and time-dependent density functional theory calculations, *Phys. Rev. B: Condens. Matter Mater. Phys.*, 2006, **74**, 121409.
25 S. Dutta and K. Wakabayashi, Magnetization due to localized states on graphene grain boundary, *Sci. Rep.*, 2015, **5**, 11744.
26 M. J. Bearpark, M. A. Robb, F. Bernardi and M. Olivucci, Molecular mechanics valence bond methods for large active spaces. Application to conjugated polycyclic hydrocarbons, *Chem. Phys. Lett.*, 1994, **217**, 513–519.
27 G. Trtaquier, N. Suaud and J. P. Malrieu, Theoretical design of high-spin polycyclic hydrocarbons, *Chem. – Eur. J.*, 2010, **16**, 8762–8772.
28 M. Melle-Franco, Uthrene, a radically new molecule?, *Chem. Commun.*, 2015, **51**, 5387–5390.
29 A. Das, T. Müller, F. Plasser and H. Lischka, Polyradical Character of Triangular Non-KekuléStructures, Zethrenes, p-Quinodimethane-Linked Bisphenalenyl, and the Clar Goblet in Comparison: An Extended Multireference Study, *J. Phys. Chem. A*, 2016, **120**, 1625–1636.
30 R. Martinazzo, S. Casolo and G. F. Tantardini, in *Physics and Applications of Graphene*, ed. S. Mikhailov, IntechOpen, Rijeka, 2011, ch. 3.
31 H. Lee, K. Paeng and I. S. Kim, A review of doping modulation in graphene, *Synth. Met.*, 2018, **244**, 36–47.
32 L. S. Panchakarla, K. S. Subrahmanyam, S. K. Saha, A. Govindaraj, H. R. Krishnamurthy, U. V. Waghmare and C. N. R. Rao, Synthesis, Structure, and Properties of Boron- and Nitrogen-Doped Graphene, *Adv. Mater.*, 2009, **21**, 4726–4730.
33 L. Ci, L. Song, C. Jin, D. Jariwala, D. Wu, Y. Li, A. Srivastava, Z. F. Wang, K. Storr, L. Balicas, F. Liu and P. M. Ajayan, Atomic layers of hybridized boron nitride and graphene domains, *Nat. Mater.*, 2010, **9**, 430.
34 R. B. Pontes, A. Fazzio and G. M. Dalpian, Barrier-free substitutional doping of graphene sheets with boron atoms: *ab initio* calculations, *Phys. Rev. B: Condens. Matter Mater. Phys.*, 2009, **79**, 033412.
35 B. Guo, Q. Liu, E. Chen, H. Zhu, L. Fang and J. R. Gong, Controllable N-Doping of Graphene, *Nano Lett.*, 2010, **10**, 4975–4980.
36 J. C. Johannsen, *et al.*, Tunable Carrier Multiplication and Cooling in Graphene, *Nano Lett.*, 2015, **15**, 326–331.
37 S. Casolo, R. Martinazzo and G. F. Tantardini, Band Engineering in Graphene with Superlattices of Substitutional Defects, *J. Phys. Chem. C*, 2011, **115**, 3250–3256.
38 Y. Zhao and D. G. Truhlar, The M06 suite of density functionals for main group thermochemistry, thermochemical kinetics, noncovalent interactions, excited states, and transition elements: two new functionals and systematic testing of four M06-class functionals and 12 other function, *Theor. Chem. Acc.*, 2008, **120**, 215–241.
39 D. Casanova and M. Head-Gordon, Restricted active space spin-flip configuration interaction approach: theory, implementation and examples, *Phys. Chem. Chem. Phys.*, 2009, **11**, 9779–9790.
40 D. Casanova, Avoided crossings, conical intersections, and low-lying excited states with a single reference method: the restricted active space spin-flip configuration interaction approach, *J. Chem. Phys.*, 2012, **137**, 084105.
41 D. Casanova, Efficient implementation of restricted active space configuration interaction with the hole and particle approximation, *J. Comput. Chem.*, 2013, **34**, 720–730.
42 S. Das, T. S. Herng, J. Zafra, P. M. Burrezo, M. Kitano, M. Ishida, T. Y. Gopalakrishna, P. Hu, A. Osuka, J. Casado, J. Ding, D. Casanova and J. Wu, Fully Fused Quinoidal/Aromatic Carbazole Macrocycles with Poly-radical Characters, *J. Am. Chem. Soc.*, 2016, **138**, 7782–7790.
43 R. Huang, H. Phan, T. S. Herng, P. Hu, W. Zeng, S.-q. Dong, S. Das, Y. Shen, J. Ding, D. Casanova and J. Wu, Higher Order π-Conjugated Polycyclic Hydrocarbons with Open-Shell Singlet Ground State: Nonazethrene *versus* Nonacene, *J. Am. Chem. Soc.*, 2016, **138**, 10323–10330.
44 M. Desroches, P. Mayorga Burrezo, J. Boismenu-Lavoie, M. Peña Álvarez, C. J. Gómez-Garca, J. M. Matxain, D. Casanova and J.-F. Morin, Casado, J. Breaking Bonds and Forming Nanographene Diradicals with Pressure, *Angew. Chem., Int. Ed.*, 2017, **56**, 16212–16217.
45 X. Lu, S. Lee, Y. Hong, H. Phan, T. Y. Gopalakrishna, T. S. Herng, T. Tanaka, M. E. Sandoval-Salinas, W. Zeng, J. Ding, D. Casanova, A. Osuka, D. Kim and J. Wu, Fluorenyl

Based Macrocyclic Polyradicaloids, *J. Am. Chem. Soc.*, 2017, **139**, 13173–13183.

46 A. Pérez-Guardiola, M. E. Sandoval-Salinas, D. Casanova, E. San-Fabián, A. J. Pérez-Jiménez and J. C. Sancho-Garca, The role of topology in organic molecules: origin and comparison of the radical character in linear and cyclic oligoacenes and related oligomers, *Phys. Chem. Chem. Phys.*, 2018, **20**, 7112–7124.

47 C. Liu, M. E. Sandoval-Salinas, Y. Hong, T. Y. Gopalakrishna, H. Phan, N. Aratani, T. S. Herng, J. Ding, H. Yamada, D. Kim, D. Casanova and J. Wu, Macrocyclic Polyradicaloids with Unusual Super-ring Structure and Global Aromaticity, *Chem*, 2018, **4**, 1586–1595.

48 Y. Ni, M. E. Sandoval-Salinas, T. Tanaka, H. Phan, T. S. Herng, T. Y. Gopalakrishna, J. Ding, A. Osuka, D. Casanova and J. Wu, [*n*]*cyclo-para*-Biphenylmethine Polyradicaloids: [*n*]Annulene Analogs and Unusual Valence Tautomerization, *Chem*, 2019, **5**, 108–121.

49 A. Pérez-Guardiola, R. Ortiz-Cano, M. E. Sandoval-Salinas, J. Fernández-Rossier, D. Casanova, A. J. Pérez-Jiménez and J. C. Sancho-Garca, From cyclic nanorings to single-walled carbon nanotubes: disclosing the evolution of their electronic structure with the help of theoretical methods, *Phys. Chem. Chem. Phys.*, 2019, **21**, 2547–2557.

50 S. Grimme and A. Hansen, A Practicable Real-Space Measure and Visualization of Static Electron-Correlation Effects, *Angew. Chem., Int. Ed.*, 2015, **54**, 12308–12313.

51 C. A. Bauer, A. Hansen and S. Grimme, The Fractional Occupation Number Weighted Density as a Versatile Analysis Tool for Molecules with a Complicated Electronic Structure, *Chem. – Eur. J.*, 2017, **23**, 6150–6164.

52 M. Head-Gordon, Characterizing unpaired electrons from the one-particle density matrix, *Chem. Phys. Lett.*, 2003, **372**, 508–511.

53 Y. Shao, *et al.*, Advances in molecular quantum chemistry contained in the Q-Chem 4 program package, *Mol. Phys.*, 2015, **113**, 184–215.

54 L. S. Bartell, Molecular geometry: bonded *versus* nonbonded interactions, *J. Chem. Educ.*, 1968, **45**, 754.

55 H. A. Jahn, Stability of Polyatomic Molecules in Degenerate Electronic States. II. Spin Degeneracy, *Proc. R. Soc. A*, 1938, **164**, 117–131.

56 R. G. Pearson, Symmetry rule for predicting molecular structures, *J. Am. Chem. Soc.*, 1969, **91**, 4947–4955.

57 I. B. Bersuker, Modern Aspects of the Jahn–Teller Effect Theory and Applications To Molecular Problems, *Chem. Rev.*, 2001, **101**, 1067–1114.

